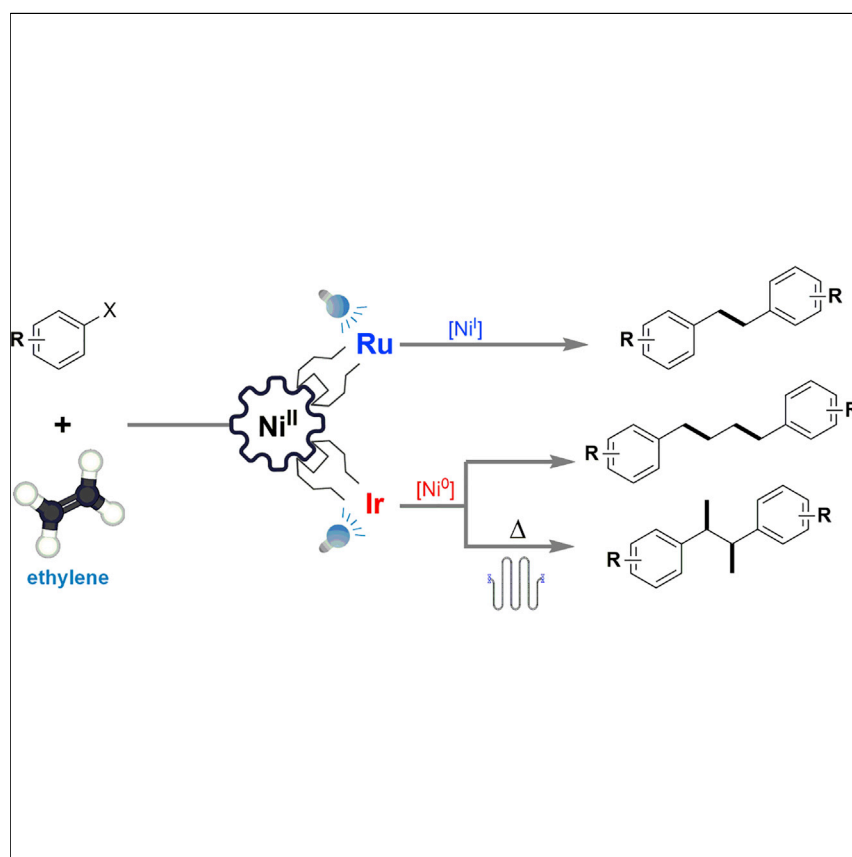


Article

Photoredox-Catalysis-Modulated, Nickel-Catalyzed Divergent Difunctionalization of Ethylene



Functionalization of ethylene without polymerization is challenging under photo-irradiation conditions. We have demonstrated that the photo-transformation of ethylene can be controllable by merging photoredox and transition-metal catalysis. In our study, the use of different photoredox catalysts was able to modulate the oxidation state of the nickel catalyst. Through different oxidation states, the nickel-catalyzed couplings proceeded via distinct pathways to generate divergent ethylene difunctionalization products selectively from the same feedstock.

Jiesheng Li, Yixin Luo, Han Wen
Cheo, Yu Lan, Jie Wu

lanyu@cqu.edu.cn (Y.L.)
chmjie@nus.edu.sg (J.W.)

HIGHLIGHTS

Photo-mediated selective
divergent difunctionalization of
ethylene with aryl halide

Modulation of Ni catalyst
oxidation states via photoredox
catalysts

Mechanistic studies supported by
DFT calculations

Inexpensive and readily available
feedstocks



Article

Photoredox-Catalysis-Modulated, Nickel-Catalyzed Divergent Difunctionalization of Ethylene

Jiesheng Li,¹ Yixin Luo,² Han Wen Cheo,¹ Yu Lan,^{2,*} and Jie Wu^{1,3,*}

SUMMARY

Divergent synthesis represents a powerful strategy for directly accessing different molecular scaffolds originating from the same starting materials. Access to different end products via transition-metal catalysis is conventionally achieved by ligand control. We herein demonstrate the use of ethylene feedstock and commercially available aryl halides to accomplish the divergent synthesis of 1,2-diarylethanes, 1,4-diarylbutanes, or 2,3-diarylbutanes in a highly selective fashion through the synergistic combination of nickel and photoredox catalysis. Mechanistic studies suggest that the observed selectivity was due to different active states of Ni(I) and Ni(0) modulated by Ru- and Ir-based photoredox catalysts, respectively. The ability to access different organometallic oxidation states via photoredox catalysis promises to inspire new perspectives for synergistic transition-metal-catalyzed divergent synthesis.

INTRODUCTION

Development of catalytic methodology to selectively produce targeted products is of essential focus in organic synthesis. In this regard, divergent synthesis serves as an appealing yet challenging strategy to selectively access multiple scaffolds starting from the same materials.^{1,2} Subtle variations on catalysts, additives, solvents, or temperature can account for distinct reaction pathways. In particular, transition-metal catalysts have conventionally relied on the proper choice of ligands bearing different electronic or steric properties to achieve divergent reactivity from the same starting materials (Figure 1A).^{3,4}

As the simplest alkene, ethylene is widely utilized in the chemical industry, with an estimated annual global production over 150 million tons, far exceeding that of any other organic compound.⁵ The high-volume usage of ethylene in industry includes the production of polyethylene materials and other commodities and feedstocks, such as ethylene oxide, propionic acid, acetaldehyde, and ethylbenzene.⁶ However, relatively few methods used ethylene as a reactant for the synthesis of fine chemicals, probably due to its inherent simplicity resulting in molecules of modest complexity and the apprehensions of handling such flammable gas. Existing catalytic transformations of ethylene into fine chemicals are typically limited to monofunctionalization, including Heck or reductive-Heck-type reactions, hydroacylations, hydrovinylation, Wacker oxidations, enyne metathesis, and ethenolysis (Figure 1B).⁷ To achieve effective ethylene difunctionalization, there is a need to avoid potential competing side reactions, such as polymerization and oligomerization, in the presence of excess ethylene⁸ or β -hydride elimination of *in-situ*-formed alkyl metallic intermediates to give unwanted Heck-type products. In this regard,

The Bigger Picture

Divergent synthesis that enables a catalytic reaction to selectively produce different products from common substrates will allow the charting of wider chemical space and the unveiling of distinct mechanistic paradigms. A common strategy for it employs different ligands to modulate organometallic catalysts. Dramatic developments in photocatalysis have enabled previously inaccessible transformations. In particular, photoredox catalysis modulates the oxidation state of transition-metal complexes, offering enormous opportunities for methodology development. Herein, we developed a photo-mediated divergent ethylene difunctionalization via modulating oxidation states of the nickel catalyst by using different photoredox catalysts. This work will inspire new perspectives for value-added chemical synthesis using ethylene as a feedstock and shed light on photoredox-catalyst-based divergent synthesis, which fundamentally differs from ligand-controlled transition-metal catalysis.

Sigman and coworkers have pioneered the palladium-catalyzed ethylene difunctionalization providing 1,1-arylvinylation⁹ and 1,1-diarylation products.^{10,11} In 2015, the Ogoshi group disclosed a 1,2-carbodifunctionalization of ethylene via a selective cross-trimerization of tetrafluoroethylene, ethylene, and aldehydes.¹² Recently, Bower and Russell reported an oxidative ethylene 1,2-difunctionalization via gold-catalyzed oxyarylation.¹³ Despite these elegant developments, effective catalytic strategies for difunctionalization of ethylene remain scarce and are highly desirable.

Visible-light photocatalysis has emerged as a powerful technique for organic synthesis over the past decade.^{14,15} In particular, the synergistic combination of photoredox catalysis and transition-metal catalysis provides distinct modes for activation of the organometallic complexes through single-electron transfer (SET) or energy transfer.¹⁶ However, to the best of our knowledge, modulating oxidation state of organometallic catalysts by photoredox catalysts to access different catalytic pathways leading to divergent products has not been previously reported. This strategy fundamentally differs from ligand-controlled transition-metal catalysis.¹⁷ Additionally, literature reports on photo-mediated transformations involving gaseous reagents are limited.^{18–22} Our group has recently developed a “stop-flow” micro-tubing (SFMT) reactor for efficient screening of gas-involved photo-mediated transformations in a convenient and safe manner.²³ As part of our ongoing interests in developing visible-light-promoted transformations using inexpensive gaseous feedstocks,^{23–25} we herein report the light-mediated ethylene difunctionalization through the synergistic combination of photoredox and Ni catalysis. Assisted by photocatalysts with different redox potentials, Ni-catalyzed reductive coupling between aryl halides and ethylene produced 1,2-diarylethanes, 1,4-diarylbutanes, and 2,3-diarylbutanes in a highly selective manner (Figure 1C).

RESULTS AND DISCUSSION

Condition Exploration for Divergent Difunctionalization of Ethylene

Earth-abundant Ni catalysts were selected for the investigation because of their intriguing properties: (1) readily accessible multiple oxidation states, (2) favorable binding with olefins, (3) difficult-to-trigger β -hydride elimination,²⁶ and (4) privilege in merging with photoredox catalysis.^{16,27,28} We commenced our study by evaluating visible-light-promoted difunctionalization of ethylene with 4-iodotoluene **1a** as the model substrate. Through the synergistic merger of a photocatalyst and a Ni catalyst, three different types of products, including one ethylene insertion product **2a**, two ethylene insertion linear product **3a**, and two ethylene insertion branched product **4a**, were generated. After extensive evaluation of reaction parameters (Figure 2 and Tables S1–S16), all three types of products could be achieved in high selectivity from identical starting materials. As shown in Figure 2, 1,2-diarylethane **2a** was obtained in 90% yield with high selectivity (**2a:3a** = 13:1) in the presence of Ru(bpy)₃Cl₂ (0.5 mol %), NiCl₂.glyme (10 mol %), *N,N,N',N'*-tetramethylethylenediamine (TMEDA) (2 equiv), and Hünig's base (2 equiv) in DMSO (0.2 M) under blue light-emitting diode (LED) irradiation at 50°C for 24 hr (entry 1, condition A). On the other hand, **3a** could be prepared in excellent selectivity and yield (90%, **2a:3a** = 1:30) using [Ir(ppy)₂(dtbbpy)]PF₆ (1 mol%) as the photocatalyst in MeCN (0.05 M) at 25°C under blue LED irradiation (entry 6, condition B). Increasing the reaction temperature to 100°C and replacing NiCl₂.glyme with NiI₂ in DMSO (0.1 M) delivered **4a** exclusively in high yield (entry 8, condition C). Notably, no diaryl coupling of **1a** or ethylene oligomerization was observed under these visible-light-mediated conditions. The holistic choice of photocatalysts, Ni catalysts, reaction

¹Department of Chemistry, National University of Singapore, 3 Science Drive 3, Singapore 117543, Republic of Singapore

²School of Chemistry and Chemical Engineering, Chongqing University, Chongqing 400044, P.R. China

³Lead Contact

*Correspondence: lanyu@cqu.edu.cn (Y.L.), chmjie@nus.edu.sg (J.W.)

<https://doi.org/10.1016/j.chempr.2018.10.006>

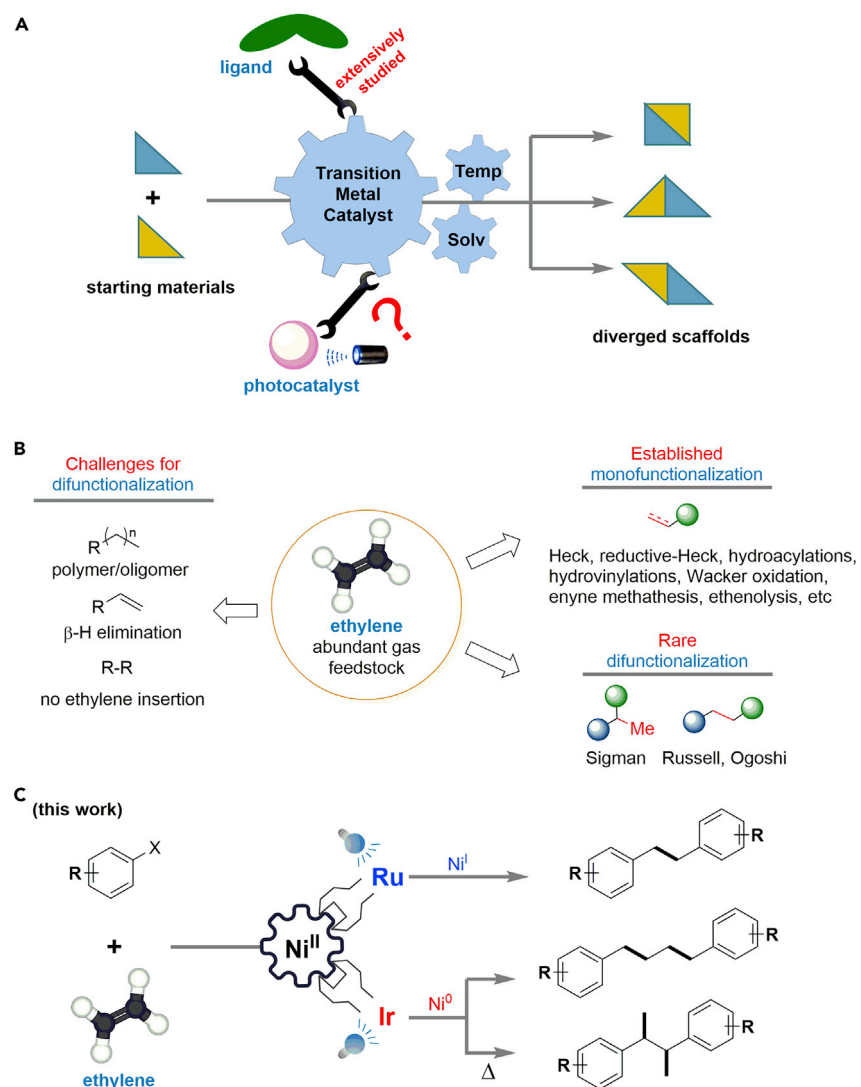


Figure 1. Divergent Functionalization of Ethylene

(A) Strategies for transition-metal-catalyzed divergent synthesis.

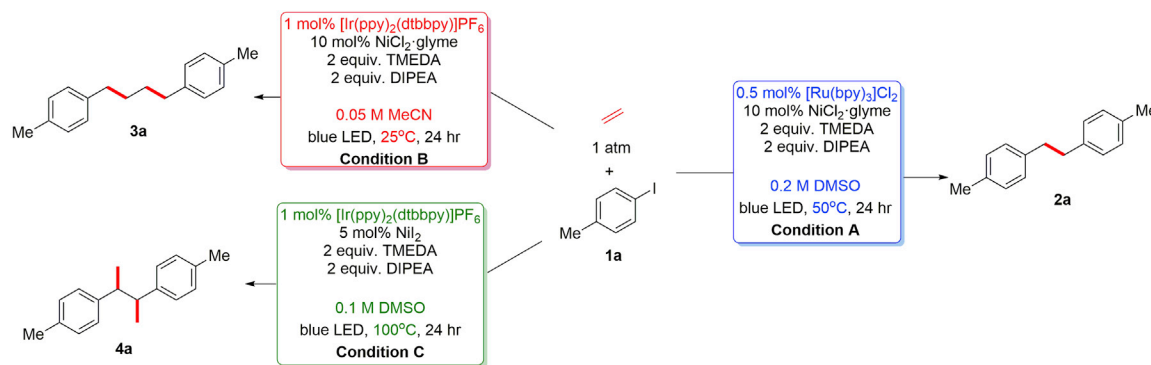
(B) Reported approaches and challenges for ethylene functionalization.

(C) Divergent and selective difunctionalization of ethylene by regulating Ni catalytic behavior with photoredox catalysts.

temperature, concentration, and solvents was critical and exhibited a profound effect on the product selectivity (Tables S1–S16).²⁹

Effect of Photoredox Catalysts

As shown in Figure 2, both $\text{Ru}(\text{bpy})_3\text{Cl}_2$ and $\text{Ru}(\text{phen})_3\text{Cl}_2$ with a similar oxidative potential ($E_{1/2}^{\text{Ru(II)/Ru(I)}} = -1.26$ V versus SCE in DMSO) could selectively produce **2a** in good selectivity and yield under condition A (entries 1 and 3). However, when the photocatalyst was changed to $\text{Ir}(\text{dFCF}_3\text{ppy})_2(\text{dtbbpy})\text{PF}_6$ or $[\text{Ir}(\text{ppy})_2(\text{dtbbpy})]\text{PF}_6$, the selectivity decreased with more 1,4-diarylbutane **3a** generated (entries 4 and 5). In addition, increasing the $\text{Ru}(\text{bpy})_3\text{Cl}_2$ catalyst loading from 0.5 mol% to 1 mol% dramatically eroded the selectivity of **2a** (entry 2). Conversely, the use of $[\text{Ir}(\text{ppy})_2(\text{dtbbpy})]\text{PF}_6$ under condition B delivered product **3a** in excellent selectivity, whereas $\text{Ru}(\text{bpy})_3\text{Cl}_2$ gave low selectivity between **2a** and **3a** (entries 6 and 7).



Entry	Condition	Photo-Catalyst	2a:3a:4a	Yield(%)	Entry	Condition	Ni-Catalyst	2a:3a:4a	Yield(%)
1	A	[Ru(bpy) ₃]Cl ₂ (0.5 mol%)	13 : 1 : 0	90	10	A	NiCl ₂ .glyme (5 mol%)	5 : 1 : 0	71
2	A	[Ru(bpy) ₃]Cl ₂ (1 mol%)	2.2 : 1 : 0	91	11	A	NiCl ₂ .glyme (10 mol%)	13 : 1 : 0	90
3	A	[Ru(phen) ₃]Cl ₂ (0.5 mol%)	10 : 1 : 0	50	12	A	NiCl ₂ .glyme (30 mol%)	15 : 1 : 0	90
4	A	Ir(dFCF ₃ ppy) ₂ (dtbbpy)PF ₆ (0.5 mol%)	3 : 5 : 0	74	13	A	Ni(COD) ₂ (10 mol%)	0 : 0 : 1	60
5	A	[Ir(ppy) ₂ (dtbbpy)]PF ₆ (0.5 mol%)	1 : 4 : 1	79	14	B	NiCl ₂ .glyme (5 mol%)	1 : 9 : 0	81
6	B	[Ir(ppy) ₂ (dtbbpy)]PF ₆ (1 mol%)	1 : 30 : 0	90	15	B	NiCl ₂ .glyme (10 mol%)	1 : 30 : 0	90
7	B	[Ru(bpy) ₃]Cl ₂ (1 mol%)	2 : 3 : 0	65	16	B	Ni(COD) ₂ (10 mol%)	1 : 33 : 0	92
8	C	[Ir(ppy) ₂ (dtbbpy)]PF ₆ (1 mol%)	0 : 0 : 1	90	17	C	NiCl ₂ .glyme (10 mol%)	0 : 0 : 1	76
9	C	[Ru(bpy) ₃]Cl ₂ (1 mol%)	0 : 0 : 1	79	18	C	NiI ₂ (5 mol%)	0 : 0 : 1	90
19	C				19	C	Ni(COD) ₂ (10 mol%)	0 : 0 : 1	93
Entry	Condition	Solvent	2a:3a:4a	Yield(%)	Entry	Condition	Deviation	2a:3a:4a	Yield(%)
20	A	MeCN instead of DMSO	2 : 1 : 0	79	26	A	0.05 M instead of 0.2 M	3 : 1 : 0	87
21	B	DMSO instead of MeCN	1 : 4 : 0	21	27	B	0.2 M instead of 0.05 M	1 : 3 : 0	81
22	C	MeCN instead of DMSO	0 : 0 : 1	29	28	A or B or C	no photocatalyst or Ni or TMEDA or light	-	0
Entry	Condition	Temperature	2a:3a:4a	Yield(%)					
23	A	25°C instead of 50°C	3 : 1 : 0	83					
24	A	80°C instead of 50°C	13 : 1 : 16	90					
25	B	60°C in 0.1 M DMSO	1 : 3 : 2	81					

Figure 2. Condition Evaluation for Visible-Light-Driven Difunctionalization of Ethylene

Ratios of **2a:3a:4a** were determined by gas chromatography analysis of crude reaction mixtures. The yields listed are the combined isolated yields, and the diastereomeric ratio (d.r.) of **4a** = 1:1. The reaction for entry 22 was conducted in the stop-flow microtubing reactor at 250 psi pressure. TMEDA, *N,N,N',N'*-tetramethylethylenediamine; DIPEA, *N,N*-diisopropylethylamine.

Notably, both Ir and Ru photocatalysts could explicitly deliver **4a** at 100°C under condition C, albeit in lower yield using the Ru system (entries 8 and 9). Even though the correlation of the photocatalyst and the product selectivity between **2a** and **3a** is still not fully understood at the current stage, and requires further investigation, we did observe that the Ru catalyst favored the formation of product **2a** while the Ir catalyst had a strong tendency toward **3a**.

Effect of Ni Catalysts

A Ni concentration dependence was observed in both selective formations of **2a** and **3a**. A higher catalyst loading of NiCl₂.glyme resulted in an improved selectivity of **2a** under condition A (entries 10–12) and **3a** under condition B (entries 14 and 15), which suggested that both catalytic processes might involve a bi-Ni-species interaction. Reaction using Ni(COD)₂ in place of NiCl₂.glyme gave no desired product **2a** under condition A (entry 13), indicating that Ni(0) might not be operative in the active catalytic cycle. In contrast, product **3a** was generated in high yield using Ni(COD)₂ under condition B (entry 16). Using NiCl₂.glyme at 100°C under condition C led to

a very high selectivity of **4a**, with 4-chlorotoluene as the sole side product (entry 17). Replacing $\text{NiCl}_2 \cdot \text{glyme}$ with NiI_2 avoided halogen exchange of **1a** (entry 18). $\text{Ni}(\text{COD})_2$ was also applicable to selectively prepare **4a** (entry 19).

Effect of Solvent

The formation of **2a** could only be achieved in DMSO or MeCN under condition A (Table S14), and MeCN resulted in much lower selectivity than DMSO (Figure 2, entry 20). Product **3a** could be generated under condition B with other polar solvents such as DMSO, dimethylformamide (DMF), and *N*-methyl-2-pyrrolidone (NMP) (Table S15). However, these solvents were incomparable with MeCN for the selective preparation of **3a**, resulting in lower yield or selectivity. The different selectivity may be attributed to the change of redox potentials of photocatalysts when in different solvents. The formation of **4a** under condition C was more tolerant toward different solvents, as polar solvents such as DMSO, MeCN, DMF, dimethylacetamide, and NMP could all produce **4a** exclusively (Table S16).

Effect of Temperature and Concentration

Temperature of 50°C and 0.2 M concentration were the optimum criteria for the selective generation of **2a** under condition A. Decreasing the reaction temperature to 25°C or lowering concentration to 0.05 M resulted in lower product selectivity (Figure 2, entries 23 and 26), whereas increasing reaction temperature to 80°C afforded **2a** and a significant amount of 2,3-diarylbutane **4a** (entry 24). The formation of **3a** under condition B proceeded selectively at 25°C and 0.05 M concentration. Increasing reaction temperature and concentration resulted in higher yield of **2a** and **4a** (entries 25 and 27). Further increasing the reaction temperature to 100°C delivered **4a** exclusively in high yield. The selectivity between **2a** and **3a** may be attributed to the varying amount of ethylene in the reaction solution at different temperature and concentration. **4a** was selectively generated above 100°C.

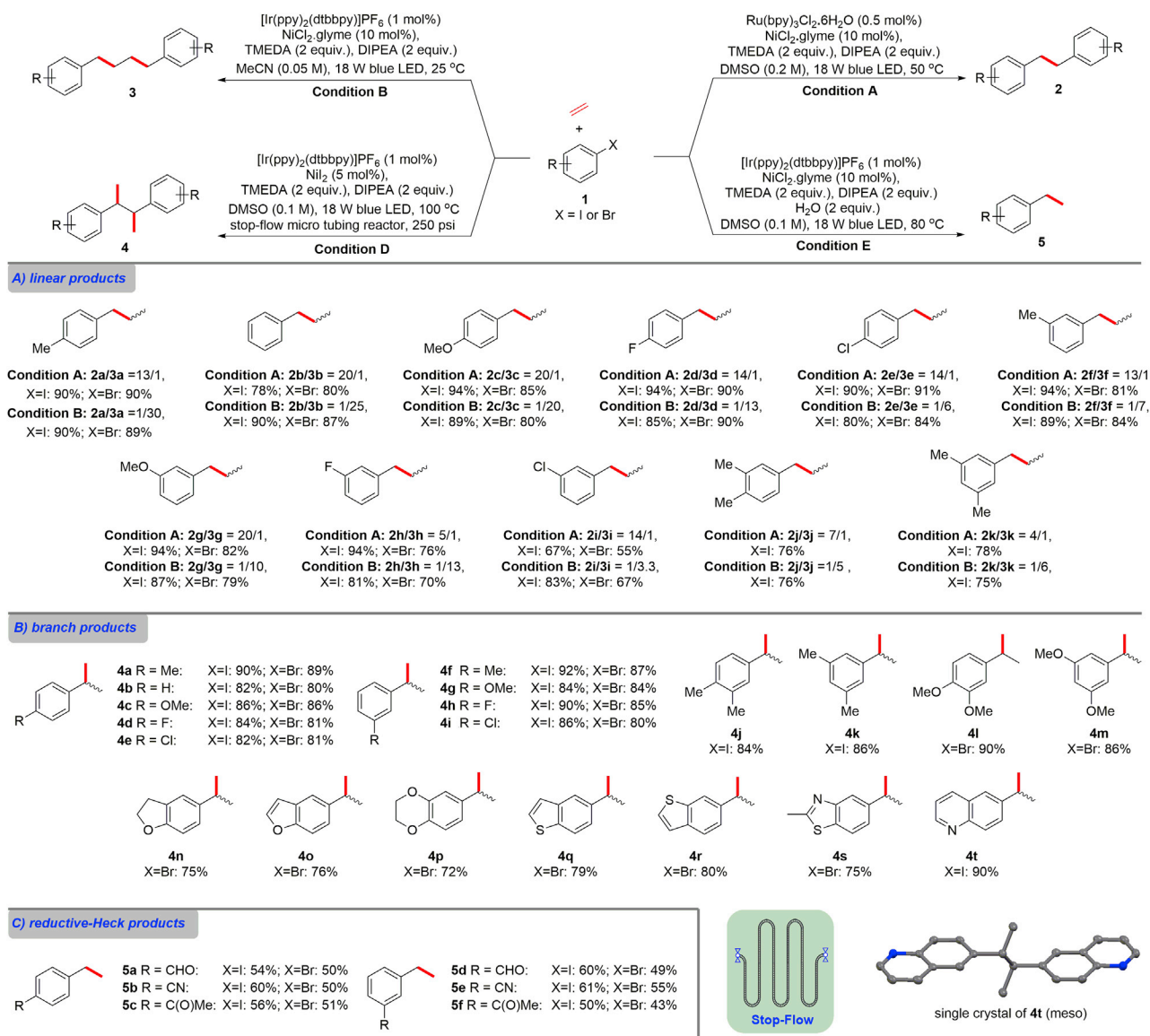
Effect of Base and Others

Hünig's base could be replaced by Et_3N , whereas other bases investigated were not effective (Tables S8–S10). Omission or decreased loading of Hünig's base led to lower productivity for compounds **2a**, **3a**, and **4a** (Tables S11–S13). Finally, no product was detected in the absence of either photocatalyst, Ni catalyst, TMEDA, or light, demonstrating the need for all these components (entry 28).²⁹ Excess TMEDA was required, which served not only as a critical ligand for Ni but also as a "sink" for the halide leaving groups. The formation of TMEDAH-I salts between protonated TMEDA and the halide were detected and characterized by X-ray crystallographic analysis (see Data and Software Availability).

Reaction Scope Investigation

As outlined in Scheme 1A, *para*- and *meta*-substituted aryl iodides and bromides with either electron-rich or electron-poor functionality could effectively react with ethylene in the presence of Ru/Ni or Ir/Ni dual catalysts under blue LED irradiation to furnish either one ethylene or two ethylene linear insertion products (**2** or **3**) in good yield and selectivity. However, both transformations were drastically affected by steric effects, as *ortho*-substituted aryl halides reacted sluggishly.

The initial substrate expansion of 2,3-diarylbutane product **4** using condition C was only applicable toward *para*-functionalized bromo- and iodoarenes, and other arene and heteroarene variants afforded either no reactivity or dehalogenation byproducts. Our speculation was that most ethylene escaped out from DMSO solution at



Scheme 1. Scope of Visible-Light-Driven Divergent Ethylene Difunctionalization

All reactions were conducted under optimized conditions; see the [Supplemental Information](#) for details of conditions A, B, D, and E. Reported yields were isolated yields. Ratios of 2:3 were determined by ^1H NMR of isolated product mixtures, except where otherwise noted. Ratios of 2a:3a were determined by gas chromatography analysis of crude reaction mixtures. The d.r. for branched product **4** = 1:1 (meso:d) as determined by ^1H NMR spectrum analysis.

100 °C in batch reactors. The SFMT reactor was thus applied to keep ethylene in the reaction solution at high temperature and high pressure for the substrate scope evaluation of **4** (condition D).²³ The SFMT reactor proved to be efficient for the generation of 2,3-diarylbutanes (**4a–4m**) from a wide range of *para*- or *meta*-substituted aryl iodides and bromides (Scheme 1B). Further substrate expansion to arene-fused heterocycles was investigated, and **4n–4t** were generated effectively. The structure of **4t** was confirmed by single-crystal structural analysis, and other products **4** were assigned by analogy. Finally, reductive-Heck products **5a–5f** were generated when arenes bearing electron-deficient substituents were subjected

to the Ir/Ni dual catalytic system under blue LED irradiation at 80°C in the presence of water (condition E).

Mechanistic Elucidation with Supporting Evidence

Reaction discovery studies suggested that the utilization of $[\text{Ir}(\text{ppy})_2(\text{dtbbpy})]\text{PF}_6$, a dilute reaction mixture, and reaction at 25°C would favor the generation of two ethylene insertion product **3**, whereas the use of $\text{Ru}(\text{bpy})_3\text{Cl}_2$, a concentrated reaction mixture, and slight heating at 50°C would prefer the formation of one ethylene insertion product **2**. In addition, the use of $[\text{Ir}(\text{ppy})_2(\text{dtbbpy})]\text{PF}_6$ at high temperature (100°C), would selectively generate two ethylene insertion branched product **4**. A critical question raised by these studies relates to tuning reaction conditions resulting in divergent products initiated by the same aryl halide and ethylene.

Selective Generation of **2** (Catalytic Cycle A)

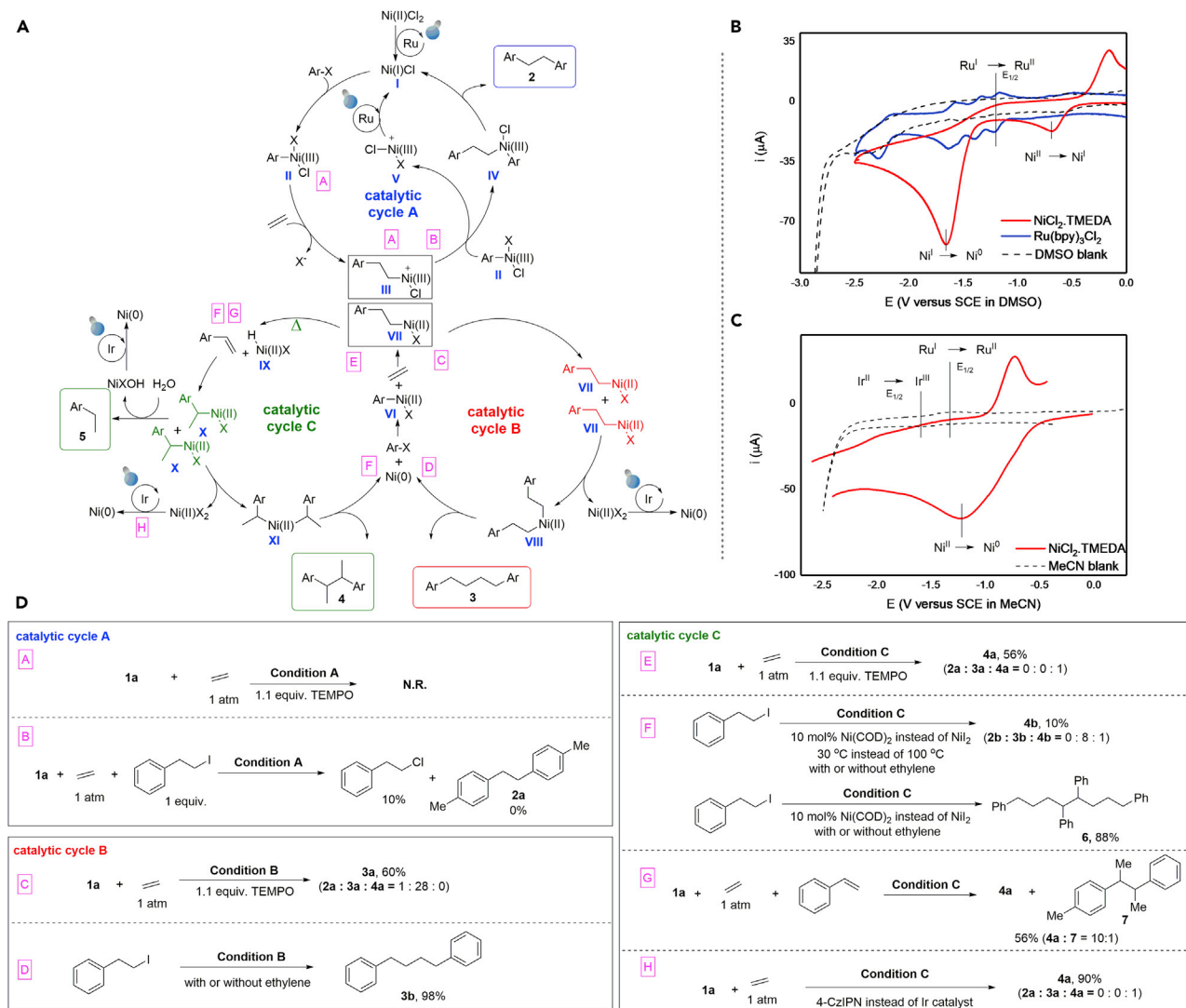
Control experiments and cyclic voltammetry (CV) analysis suggested Ni(I) as the active catalyst for the generation of 1,2-diarylethane **2** in the Ru/Ni dual catalyst system.^{30,31} CV analysis of NiCl_2 -TMEDA complex ($E_{\text{p}}^{\text{Ni(II)/Ni(I)}} = -0.68$ V and $E_{\text{p}}^{\text{Ni(I)/Ni(0)}} = -1.66$ V versus SCE in DMSO) and $\text{Ru}(\text{bpy})_3\text{Cl}_2$ ($E_{1/2}^{\text{Ru(I)/Ru(II)}} = -1.26$ V versus SCE in DMSO), where Ru(I) can partially reduce Ni(II) to Ni(I) with roughly 0.58 V of thermodynamic driving force, while full reduction of Ni(II) to Ni(0) is unfavorable with roughly -0.40 V (Scheme 2B and Figures S22–S25). These data are in accordance with the reducing ability of $\text{Ru}(\text{bpy})_3\text{Cl}_2$, which is inefficient in conjunction with an amine sacrificial reductant for Ni-catalyzed reductive coupling reactions.^{32,33} The reaction was totally suppressed in the presence of stoichiometric TEMPO (Scheme 2D [A]). Furthermore, no ethylene insertion product was observed when equal molarities of **1a** and 2-iodoethylbenzene were added (Scheme 2D [B]). This could indicate a better reactivity of alkyl iodide than of aryl iodide toward the *in situ* generated Ni(I) species and that ethylene insertion into alkyl Ni intermediate may be difficult. Intriguingly, reaction in MeCN resulted in a significant amount of **3a** (**2a**:**3a** = 2:1; Figure 2, entry 20). This was probably due to the similar reduction potential of $\text{Ru}(\text{bpy})_3\text{Cl}_2$ in MeCN ($E_{1/2}^{\text{Ru(I)/Ru(II)}} = -1.33$ V versus SCE) versus Ni(II) to Ni(0) ($E_{\text{p}} = -1.27$ V versus SCE in MeCN) as illustrated in Scheme 2C, where $\text{Ru}(\text{bpy})_3\text{Cl}_2$ was capable of fully reducing Ni(II) to Ni(0), thereby altering the selectivity.³⁴ Lastly, light on/off experiments indicated that light was essential for this transformation (Figure S9).

Selective Generation of **3** (Catalytic Cycle B)

CV analysis indicated that $[\text{Ir}(\text{ppy})_2(\text{dtbbpy})]\text{PF}_6$ ($E_{1/2}^{\text{Ir(II)/Ir(III)}} = -1.51$ V versus SCE in MeCN) gave roughly 0.24 V of thermodynamic driving force to fully reduce Ni(II) complex to Ni(0) ($E_{\text{p}} = -1.27$ V versus SCE in MeCN; Scheme 2C), which indicated that Ni(0) was involved in the formation of **3a**. The reaction proceeded to afford **3a** in the presence of 1.1 equiv TEMPO (Scheme 2D [C]), suggesting a non-radical pathway. Starting with 2-iodoethylbenzene instead of 4-iodotoluene **1a** exclusively generated homo-dimerization product **3b** (Scheme 2D [D]). The absence of ethylene insertion again suggested that the transient alkyl Ni intermediate might not undergo migratory insertion with ethylene, thus preventing ethylene oligomerization and polymerization.

Selective Generation of **4** (Catalytic Cycle C)

Prevailing mechanistic studies indicates that Ni(0) will be generated with Ir-photocatalyst. Radical may not be involved in the catalytic cycle as desired product **4a** was generated in the presence of 1.1 equiv TEMPO (Scheme 2D [E]). **4b** could be obtained when 2-iodoethylbenzene instead of 4-iodotoluene **1a** was used in the



Scheme 2. Proposed Mechanisms with Supporting Evidence

- (A) Proposed plausible mechanisms. Photo-reductive quenching cycle was omitted for clarity; see Figures S18–S20 for detail mechanisms of each cycle.
 (B) Cyclic voltammetry analysis of Ni catalyst and Ru photocatalyst in DMSO.
 (C) Cyclic voltammetry analysis of Ni catalyst, Ru and Ir photocatalysts in MeCN.
 (D) Control experiments to elucidate the mechanisms.

presence of $\text{Ni}(\text{COD})_2$ catalyst at 30°C (Scheme 2D [F] and Figure S11), which supported that the isomerization of alkyl Ni intermediate through β -hydride elimination to generate nickel hydride was possible even at room temperature to deliver branched product 4. Surprisingly, increasing temperature to 100°C exclusively delivered tetramer 6, which indicated that the *in situ* generated nickel hydride would preferentially undergo reductive elimination in the presence of amine base instead of re-inserting back onto styrene (see Figure S13 for proposed mechanism). Further investigations are underway to explore this unprecedented transformation. In addition, the nickel hydride species was capable of intercepting another olefin present in the reaction mixture (Scheme 2D [G] and Figure S12).³⁵ Finally, organo-photocatalyst 1,2,3,5-tetrakis(carbazol-9-yl)-4,6-dicyanobenzene (4CzIPN)³⁶ could be applied to replace the Ir catalyst to enable a more economical transformation

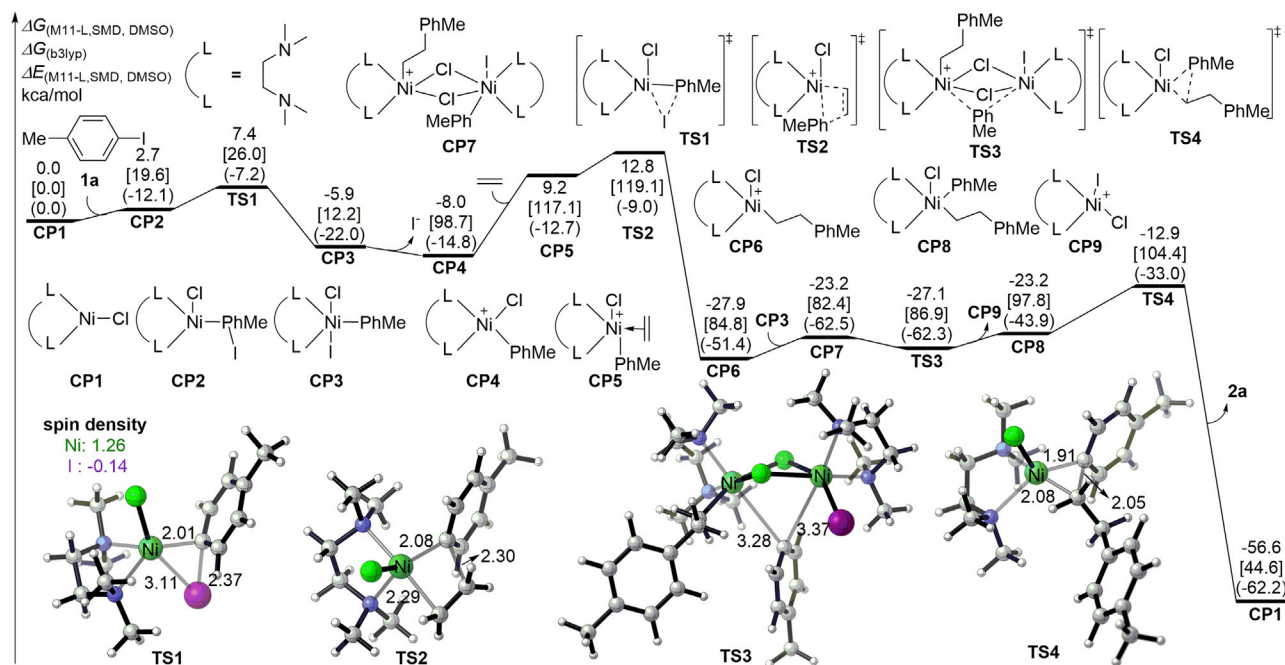


Figure 3. Free-Energy Profiles for the Ni(I)-Ni(III) Catalytic Cycle of the Diarylethane Product 2a Generation Process

Values for bond lengths are given in angstroms.

(Scheme 2D [H]). Deuteration experiments suggested that the mechanism for the generation of product 5 was built on catalytic cycle C, where alkyl Ni was quenched by D₂O instead of DMSO after isomerization (Figure S14).

To further reveal the Ni(I)-based mechanistic pathway for the selective generation of diarylethane product 2, density functional theory (DFT) method M11-L was applied. As shown in Figure 3, the active catalyst Ni(I) species CP1 was chosen as the relative zero point for the free energy profiles, which could be generated via SET with reduced photocatalyst Ru(bpy)₃⁺ (a detailed mechanism is shown in Figure S18). The generation of an aryl radical via Ni(I)-induced SET oxidative addition was ruled out as the relative free energy was too high (50.2 kcal/mol; Figure S16). 4-Iodotoluene 1a was thus activated by coordinating with CP1 to give the intermediate CP2 with a free energy increase of 2.7 kcal/mol. The subsequent oxidative addition occurred via a three-membered ring transition state TS1 with a 7.4 kcal/mol overall barrier, where an aryl-Ni(III) complex CP3 was generated. The geometry of TS1 is shown in Figure 3, in which the Ni-I distance (3.11 Å) was shorter than the sum of their van der Waals radii. The calculated spin density of this transition state illustrated that the unpaired electrons were mainly localized on the Ni atom. Further intrinsic reaction coordinate calculations demonstrated that iodide coordinated with Ni(III) to form intermediate CP3 following TS1. Then the ligand exchange with ethylene would form intermediate CP5 with 15.1 kcal/mol endergonic with the release of iodide. The irreversible migratory insertion of coordinated ethylene into aryl-Ni bond occurred via transition state TS2 with an overall barrier of 20.8 kcal/mol to form an alkyl Ni(III) intermediate CP6. The theoretical calculation revealed that the ethylene insertion step was considered to be the rate-determining step in catalytic cycle A. Further coordination of CP6 followed by insertion of another ethylene was unfavorable with a 26.6 kcal/mol endergonic barrier (Figure S17). CP6 could react with intermediate CP3 to form a dichloro-bridged binuclear Ni(III) intermediate

CP7. Then rapid intramolecular transmetallation of the aryl group could take place via TS3. The calculated barrier of this step was lower than zero, which could be attributed to the computational error of the solvation effect and the usage of entropy correction in the gas phase. The following reductive elimination could take place from a mononuclear Ni(III) intermediate CP8 with a free energy barrier of only 10.3 kcal/mol through TS4. After releasing product 2a, the active catalyst CP1 was regenerated. Moreover, the possibility for the formation of 1,4-diarylbutane 3a through the Ni(I)–Ni(III) catalytic cycle was considered theoretically (Figure S15). However, the overall activation free energy for the formation of 3a was 34.8 kcal/mol via transition state TS6, and the relative free energy was 19.8 kcal/mol higher than via TS4.

Tentative Proposed Mechanistic Cycle

In light of all the experimental data and DFT calculation, plausible mechanistic pathways for the divergent ethylene functionalization are proposed in Scheme 2A. Different from previously reported Ni(0)-catalyzed reductive coupling reactions,^{31,37} the synthesis of 1,2-diarylethane 2 (catalytic cycle A) is initiated by Ru(bpy)₃Cl₂-promoted Ni(I) formation. The generated Ni(I) intermediate I subsequently undergoes oxidative addition with aryl halides to form aryl-Ni(III) species II. Migratory insertion of ethylene into aryl-Ni(III) with the dissociation of a halide ligand (trapped by TMEDA⁺) generates a cationic alkyl Ni(III) species III. The aryl transfer by a transmetallation between III and aryl-Ni(III) species II delivers an aryl alkyl Ni(III) species IV, which can undergo a rapid reductive elimination to yield diarylethane product 2 and regenerate the active Ni(I) catalyst I. The transmetallation process would also generate a cationic Ni(III) species V, which could be reduced by a Ru-based photoredox cycle to regenerate Ni(I) I. As for Ir-catalyzed generation of 1,4-diarylbutanes 3 (catalytic cycle B), Ni(II) precursor is fully reduced to Ni(0) through the Ir-based photoredox cycle. Oxidative insertion of aryl halides to Ni(0) followed by ethylene migratory insertion furnishes alkyl Ni(II) complex VII. As suggested by control experiments, additional ethylene insertion would not occur with alkyl Ni species VII, thereby preventing unwanted oligomerization and polymerization. Transmetallation between two molecules of complex VII delivers the dialkyl Ni(II) intermediate VIII and a Ni(II) halide, the latter will be reduced by photocatalyst and amine reductant to regenerate Ni(0). Reductive elimination of VIII achieves 3 and Ni(0). In the proposed catalytic cycle C for the selective generation of 2,3-diarylbutanes 4, Ni(II) complex VII is generated via Ir-photocatalyst through a similar process as catalytic cycle B. β -Hydride elimination is triggered at high temperature to give a Ni hydride species IX, which then undergoes a reinsertion to form the more thermodynamically favored benzyl Ni intermediate X.³⁸ Transmetallation between two molecules of X followed by reductive elimination accomplishes the synthesis of 4 and regenerates the Ni(0) catalyst. Alternatively, in the presence of water, intermediate X could be quenched to deliver reductive Heck-type product 5.

Conclusion

In summary, we have discovered a divergent synthesis of 1,2-diarylethanes, 1,4-diarylbutanes, 2,3-diarylbutanes, and ethylarenes from a common aryl halide and ethylene through the synergistic combination of photoredox and Ni catalysis. All products can be generated in a highly selective fashion by proper selection of photocatalysts and tuning the reaction parameters. Various control experiments and DFT calculations were conducted to explore the mechanisms for the selective product generation. Our study showcases the difunctionalization of ethylene under photoredox conditions, which will inspire new perspectives for value-added chemical synthesis using ethylene as a feedstock. Furthermore, distinct catalytic pathways

can be obtained via photoredox modulation of organometallic intermediates to access desired oxidation states, which will shed new light on transition-metal-catalyzed divergent synthesis.

EXPERIMENTAL PROCEDURES

Full experimental procedures are provided in the [Supplemental Information](#).

DATA AND SOFTWARE AVAILABILITY

The structures of TMEDAH-I, *meso*-**4t**, and **6** reported in this article have been deposited in the Cambridge Crystallographic Data Centre under accession numbers CCDC: 1825640, 1825641, and 1825642, respectively.

SUPPLEMENTAL INFORMATION

Supplemental Information includes Supplemental Experimental Procedures, 123 figures, 38 tables, and 3 data files and can be found with this article online at <https://doi.org/10.1016/j.chempr.2018.10.006>.

ACKNOWLEDGMENTS

We are grateful for the financial support provided by the National University of Singapore and the Ministry of Education of Singapore (R-143-000-665-114 and R-143-000-696-114), GlaxoSmithKline and the Singapore Economic Development Board (R-143-000-687-592), the A*STAR RIE2020 Plan for Advanced Manufacturing and Engineering (A1783c0013), and the National Natural Science Foundation of China (21822303 and 21772020). We thank Prof. Zhu Shaolin (Nanjing University) and Dr. Yang Yang (UC-Berkeley) for their helpful discussions.

AUTHOR CONTRIBUTIONS

J.L. and H.W.C. conducted the experiments and analyzed the data. Y. Luo and Y. Lan conducted the DFT calculation and mechanism study. J.W. and J. Li designed the project, analyzed the data, and wrote the manuscript.

DECLARATION OF INTERESTS

The authors declare no competing interests.

Received: May 30, 2018

Revised: September 3, 2018

Accepted: October 11, 2018

Published: November 8, 2018

REFERENCES AND NOTES

1. Ping, L., Chung, D.S., Bouffard, J., and Lee, S.G. (2017). Transition metal-catalyzed site- and regio-divergent C–H bond functionalization. *Chem. Soc. Rev.* **46**, 4299–4328.
2. Lee, Y.C., Kumar, K., and Waldmann, H. (2018). Ligand-directed divergent synthesis of carbonyl and heterocyclic ring systems. *Angew. Chem. Int. Ed.* **57**, 5212–5226.
3. Meng, Q.Y., Wang, S., Huff, G.S., and König, B. (2018). Ligand-controlled regioselective hydrocarboxylation of styrenes with CO₂ by combining visible light and nickel catalysis. *J. Am. Chem. Soc.* **140**, 3198–3201.
4. Liu, J., Liu, Q., Franke, R., Jackstell, R., and Beller, M. (2015). Ligand-controlled palladium-catalyzed alkoxy-carbonylation of allenes: regioselective synthesis of α,β - and β,γ -unsaturated esters. *J. Am. Chem. Soc.* **137**, 8556–8563.
5. McCoy, M., Reisch, M., Tullo, A.H., Short, P.L., Tremblay, J.F., and Storck, W.J. (2006). Production: growth is the norm. *Chem. Eng. News* **84**, 59–236.
6. Independent Chemical Information Service (2007). Ethylene uses and market data. <https://www.icis.com/resources/news/2007/11/05/9075777/ethylene-uses-and-market-data>.
7. Saini, V., Stokes, B.J., and Sigman, M.S. (2013). Transition-metal-catalyzed laboratory-scale carbon–carbon bond-forming reactions of ethylene. *Angew. Chem. Int. Ed.* **52**, 11206–11220.
8. For UV-light-promoted cycloaddition and free-radical polymerization using ethylene, see Mirbach, M.F., Mirbach, M.J., and Saus, A. (1982). High-pressure photochemistry and Ultraviolet spectroscopy in gas-liquid systems. *Chem. Rev.* **82**, 59–76.
9. Saini, V., and Sigman, M.S. (2012). Palladium-catalyzed 1,1-difunctionalization of ethylene. *J. Am. Chem. Soc.* **134**, 11372–11375.

- Saini, V., Liao, L., Wang, Q., Jana, R., and Sigman, M.S. (2013). Pd(0)-catalyzed 1,1-diarylation of ethylene and allylic carbonates. *Org. Lett.* **15**, 5008–5011.
- For the first nickel-catalyzed 1,1-diarylation of ethylene, see Rollin, Y., Meyer, G., and Troupel, M. (1982). Catalyse par des complexes du nickel l'électrosynthèse de 1,1-diaryléthane à partir d'halogénures aromatiques et d'éthylène. *Tetrahedron Lett.* **23**, 3573–3576.
- Ohashi, M., Shirataki, H., Kikushima, K., and Ogoshi, S. (2015). Nickel-catalyzed formation of fluorine-containing ketones via the selective cross-trimerization reaction of tetrafluoroethylene, ethylene, and aldehydes. *J. Am. Chem. Soc.* **137**, 6496–6499.
- Harper, M.J., Emmett, E.J., Bower, J.F., and Russell, C.A. (2017). Oxidative 1,2-difunctionalization of ethylene via gold-catalyzed oxyarylation. *J. Am. Chem. Soc.* **139**, 12386–12389.
- Prier, C.K., Rankic, D.A., and MacMillan, D.W.C. (2013). Visible light photoredox catalysis with transition metal complexes: applications in organic synthesis. *Chem. Rev.* **113**, 5322–5363.
- Narayanan, J.M., and Stephenson, C.R. (2011). Visible light photoredox catalysis: applications in organic synthesis. *Chem. Soc. Rev.* **40**, 102–113.
- Twilton, J., Le, C., Zhang, P., Shaw, M.H., Evans, R.W., and MacMillan, D.W.C. (2017). The merger of transition metal and photocatalysis. *Nat. Rev. Chem.* **1**, 0052.
- Corcoran, E.B., Pirnot, M.T., Lin, S., Dreher, S.D., DiRocco, D.A., Davies, I.W., Buchwald, S.L., and MacMillan, D.W.C. (2016). Aryl amination using ligand-free Ni(II) salts and photoredox catalysis. *Science* **353**, 279–283.
- Seo, H., Katcher, M.H., and Jamison, T.F. (2017). Photoredox activation of carbon dioxide for amino acid synthesis in continuous flow. *Nat. Chem.* **9**, 453–456.
- Majek, M., and Wangelin, A.J. (2015). Metal-free carbonylations by photoredox catalysis. *Angew. Chem. Int. Ed.* **54**, 2270–2274.
- Yatham, V.R., Shen, Y., and Martin, R. (2017). Catalytic intermolecular dicarbofunctionalization of styrenes with CO₂ and radical precursors. *Angew. Chem. Int. Ed.* **56**, 10915–10919.
- Shimomaki, K., Murata, K., Martin, R., and Iwasawa, N. (2017). Visible-light-driven carboxylation of aryl halides by the combined use of palladium and photoredox catalysts. *J. Am. Chem. Soc.* **139**, 9467–9470.
- Meng, Q.-Y., Wang, S., and König, B. (2017). Carboxylation of aromatic and aliphatic bromides and triflates with CO₂ by dual visible-light-nickel catalysis. *Angew. Chem. Int. Ed.* **56**, 13426–13430.
- Xue, F., Deng, H.P., Xue, C.W., Mohamed, D.M.B., Tang, K.Y., and Wu, J. (2017). Reaction discovery using acetylene gas as the chemical feedstock accelerated by the “stop-flow” micro-tubing reactor system. *Chem. Sci.* **8**, 3623–3627.
- Hou, J., Ee, A., Feng, W., Xu, J.H., Zhao, Y., and Wu, J. (2018). Visible-light-driven alkyne hydro-/carbocarboxylation using CO₂ via iridium/cobalt dual catalysis for divergent heterocycle synthesis. *J. Am. Chem. Soc.* **140**, 5257–5263.
- Deng, H.P., Zhou, Q., and Wu, J. (2018). Micro-tubing reactor-assisted aliphatic C–H functionalization utilizing HCl as the hydrogen atom transfer catalyst precursor in conjunction with an organo photoredox catalyst. *Angew. Chem. Int. Ed.* **57**, 12661–12665.
- Tasker, S.Z., Standley, E.A., and Jamison, T.F. (2014). Recent advances in homogeneous nickel catalysis. *Nature* **509**, 299–309.
- Tellis, J.C., Kelly, C.B., Primer, D.N., Jouffroy, M., Patel, N.R., and Molander, G.A. (2016). Single-electron transmetalation via photoredox/nickel dual catalysis: unlocking a new paradigm for sp³-sp² cross-coupling. *Acc. Chem. Res.* **49**, 1429–1439.
- Deng, H.P., Fan, X.Z., Chen, Z.H., Xu, Q.H., and Wu, J. (2017). Photo-induced nickel-catalyzed chemo- and regioselective hydroalkylation of internal alkynes with ether and amide α -hetero C(sp³)-H bonds. *J. Am. Chem. Soc.* **139**, 13579–13584.
- A detailed study can be found in the Supplemental Information.
- For Ni(II)-based catalytic cycle via Ir-photoredox/Ni dual catalysis, see Oderinde, M.S., Frenette, M., Robbins, D.W., Aquila, B., and Johannes, J.W. (2016). Photoredox mediated nickel catalyzed cross-coupling of thiols with aryl and heteroaryl iodides via thiyl radicals. *J. Am. Chem. Soc.* **138**, 1760–1763.
- Oderinde, M.S., Jones, N.H., Juneau, A., Frenette, M., Aquila, B., Tentarelli, S., Robbins, D.W., and Johannes, J.W. (2016). Highly chemoselective iridium photoredox and nickel catalysis for the cross-coupling of primary aryl amines with aryl halides. *Angew. Chem. Int. Ed.* **55**, 13219–13223.
- Paul, A., Smith, M.D., and Vannucci, A.K. (2017). Photoredox-assisted reductive cross-coupling: mechanistic insight into catalytic aryl-alkyl cross-couplings. *J. Org. Chem.* **82**, 1996–2003.
- Cyclic voltammetry (CV) studies have been widely used in photoredox catalysis to elucidate the oxidation state of transition metals. However, we cannot exclude endothermic steps in catalytic cycles Studer, A., and Curran, D.P. (2016). Catalysis of radical reactions: a radical chemistry perspective. *Angew. Chem. Int. Ed.* **55**, 58–102.
- For an example of a solvent effect study in dual Ir-photoredox/Ni dual catalysis, see Oderinde, M.S., Varela-Alvarez, A., Auila, B., Robbins, D.W., and Johannes, J.W. (2015). Effects of molecular oxygen, solvent, and light on iridium-photoredox/nickel dual-catalyzed cross-coupling reactions. *J. Org. Chem.* **80**, 7642–7651.
- Chen, F., Chen, K., Zhang, Y., He, Y., Wang, Y.M., and Zhu, S. (2017). Remote migratory cross-electrophile coupling and olefin hydroarylation reactions enabled by in situ generation of NiH. *J. Am. Chem. Soc.* **139**, 13929–13935.
- Luo, J., and Zhang, J. (2016). Donor-acceptor fluorophores for visible-light-promoted organic synthesis: photoredox/Ni dual catalytic C(sp³)-C(sp²) cross-coupling. *ACS Catal.* **6**, 873–877.
- Tsou, T.T., and Kochi, J.K. (1979). Mechanism of oxidative addition. Reaction of nickel(0) complexes with aromatic halides. *J. Am. Chem. Soc.* **101**, 6319–6332.
- He, Y., Cai, Y., and Zhu, S. (2017). Mild and regioselective benzylic C–H functionalization: Ni-catalyzed reductive arylation of remote and proximal olefins. *J. Am. Chem. Soc.* **139**, 1061–1064.